Infrared Antireflection Moth's Eye Nanostructures

Megan McGuffey, Scott Roman, Luke Bittner, Yoni Griboff,
Garrett Wessler, Mariela Georgieva, John Osmond

Abstract

Biomimicry, attempting to create nanostructures that simulate those found in nature, is a relatively new field of study that is generating interest. One such natural structure that is used for antireflection applications is the moth's eye due to its excellent ability to absorb light in the visible spectra from a wide range of angles. These moth's eye nanostructures are typically made with silicon due to its low cost and the ease with which it can be etched. Silicon's bandgap of 1.3 eV makes it sufficient for solar cell applications in the visible spectra where decreasing the reflectance would improve solar cell efficiency. However, in the infrared (IR) where most wavelengths have an energy of greater than 1.3 eV, silicon becomes transparent. Because of this, materials with bandgaps higher than silicon such as indium antimonide (InSb), mercury cadmium telluride (HgCdTe), and germanium (Ge) are used for applications in the IR. Technologies such as forward looking infrared (FLIR) cameras, solar cells, and IR telescopes could benefit from having our antireflection moth's eye nanostructure.

In our project, we have created a cone-and-ball nanostructure design capable of significantly reducing reflection in the near to mid-wavelength IR. We constructed a 3D model of our nanostructure using Computer Software Technology (CST) and simulated normal incidence on our nanostructure at wavelengths between 0.75 μm and 3 μm. Initially, only silicon was used in the simulations to analyze the effectiveness of our design. Then the nanostructure was optimized for silicon in the visible spectrum and this optimized structure was simulated in the IR with satisfactory results. Next, the nanostructure was simulated and optimized for InSb, HgCdTe, and Ge in the near and short-wavelength IR. This project was completely simulation based as there was not enough time to fabricate the structure in the FabLab.

Material Science & Engineering Aspects

This project is a perfect example of the structure-processing properties relationship that is so important in the field of materials science. Specifically, the cone-and-ball design of our biomimetic moth's eye nanostructure requires precise microprocessing synthesis methods which, if done correctly, can produce the anti-reflection properties we simulated in CST. This project also involves material engineering as it requires knowledge of microprocessing, wave physics, and photonics. The cone-and-ball nanostructure design is made possible by using a self-assembling block copolymer. The benefit of using a self-assembling material is that it dramatically cuts down on the number of microprocessing steps and on the chemical waste produced during processing. It also makes the nanostructure easily tunable as different shapes and dimensions can be created just by slight changes to the chemistry of the block copolymer. The shape of the block copolymer is what determines how the nanostructure interacts with light instead of the chemical composition of the block copolymer[1]. Since the main goal of this project is optimization of a structure using frequency domain simulations, it is essential that all material properties such as the dielectric constant and refractive index are known and accurate to ensure that the simulations give accurate results.

Previous Work

With the increasing complexity of modern technology, researchers have turned toward biomimicry, or the copying of natural structures and systems, as a way of advancing technology[2]. One such structure, the eye of a moth, has garnered interest in the past decade because a moth's eye does not reflect light from most angles. Researchers soon applied the nanostructure to lowering the surface reflectance of solar cells[3]. Silicon, the primary component of most commercial solar cells, has a surface reflection of over 30%; by lowering the surface reflectance, solar cell efficiency can be further improved[4].

Previous anti-reflection technology only absorbed a limited range of wavelengths for a specific angle. In order to use this technology, the solar panel must also use a precise positioning system so it remains at the same angle to the sun[5]. In 2007, Huang et al. proposed using a periodic array of narrow silicon cones to create an anti-reflective surface capable of absorbing 90% of visible light with an angle of incidence ranging from 25 to 70 degrees[3]. Likewise, in 2009, Diedenhofen et al. created and compared the reflection of arrays of GaP nanorods and nanocones. These arrays were only about 100 nm high but displayed a reflectance 10% less than the bare substrate. They also found the nanocones displayed a slightly lower reflectance than the nanorods[6]. Park et al. and Yang et al. both created narrow silicon nanocones several hundred nanometers in height. Both groups focused on the anti-reflection properties of the nanocones but Park also tested the hydrophobicity of the nanostructure. Park found the narrow nanocones increased the transmission of the silicon from approximately 30% to 50% while Yang found that adding the nanocones reduced the peaks of the reflection efficiency from approximately 0.4 to less than 0.1[7,8]. In the following years, research groups have investigated cones and rounded rods of varying length and spacing to determine the optimum shape for visible light absorption at a large set of angles continuing to focus on improving solar cell efficiency.

In 2015, Rahman et al. investigated a new cone-and-ball structure of varying heights made of silicon and alumina. They obtained a reflectance of less than 5% for the 215 nm high nanostructure for angles of incidence approximately 10 to 60 degrees. The most notable feature of the nanostructure was that it displayed a near constant reflectance of less than 5% for the entire wavelength range measured, from 400 to 1000 nm[9]. This suggests that the absorbance of this nanostructure will remain under 10% farther into the IR range. However, little to no research has been performed in applying this nanostructure to IR wavelengths, despite many applications that would benefit from reduced IR reflectance[10].

Design Goals

For this project, we intended to design an anti-reflection cone-and-ball nanostructure able to reduce the IR reflectance of a material to below 20% for either near, short-wavelength, or mid-wavelength IR light. As described in the Previous Work section, several research groups have created either the cone structure or the cone-and-ball structure and observed reflectances of less than 10% in the visible range. While our goal of 20% reflectance was higher than reflectances already experimentally accomplished in the visible range, it is still a significant drop in the surface reflectance of many semiconductor materials (40%-60%) and accommodates for unexpected effects we might have observed when we transitioned to the IR range[11]. As part of developing the

IR antireflection design, we also intended to replicate the experimental data found in the literature to within 10% and to study the effects of applying the cone-and-ball nanostructure to IR wavelengths, as previous research has only studied the effectiveness of the cone-and-ball nanostructures in the visible spectrum. Since the bandgap of silicon is 1.3 eV, we would choose materials with a larger wavelength bandgap for our IR anti-reflection nanosurface design so any bandgap effects on the optical properties could be ignored for the scope of this project. Our final design is an optimized geometry for silicon in the visible range, as well as an optimized geometry and material choice for both near IR and short-wavelength IR applications.

Technical Approach

In this project, we optimized two aspects of our IR antireflection nanostructure: (1) geometry of the cone-and-ball nanostructures to minimize reflectance and (2) material selection to minimize reflectance in relevant wavelengths ($\lambda > 1$ μm). We numerically calculated the reflectance using the EM wave simulator CST: Microwave Studio[12]. Using CST, we achieved goal (1) of geometric optimization through a combination of parametric and optometric sweeps over the various geometric configurations. To achieve goal (2), we input various materials into our simulations and observed which materials performed best in specific wavelength regimes via optometric sweeps to minimize reflectance. While we were not able to quickly sweep over many materials in CST, we found that processibility and cost severely limited the choice of materials considered in our experiments. Due to these constraints, we identified indium antimonide (InSb), germanium (Ge), and mercury cadmium telluride (HgCdTe) as the most suitable materials due to their small band gaps and etchability[13].

As a first step, we conducted basic control simulations using a planar slab of standard materials and environment (Si, vacuum) to determine the best way to use a plane wave source. Troubleshooting this basic simulation allowed us to identify a few critical aspects to setting up a simulation template for our cone-and-ball nanostructure simulations. These aspects include using the frequency domain solver, using a hexahedral mesh, and defining proper boundary conditions. In our simulations, we were only concerned with the S_{11} output, as this is the reflectance off the structure[12]. After successfully obtaining simulation results for S_{11} that matched literature values to within 10% (shown in Figure 3), we moved toward the more complicated simulations of the IR-antireflection cone-and-ball nanostructures.

In order to run our simulations, we first needed to draw a CAD model of our cone-and-ball nanostructure. When drawing the CAD model of our nanostructure in CST, we parametrized each dimension (cone height, cone radii, cone spacing, neck thickness, and ball radius) in the simulation, as shown in Figure 1 below, so that it was easily alterable at a later point in time. This ensured that we could sweep any dimension and create a pseudo-design of experiments (DOE) type environment. We performed these DOE-type experiments to understand how changing different parameters influenced the overall reflectivity, providing us with a better sense of whether we could trust the results of the simulations.
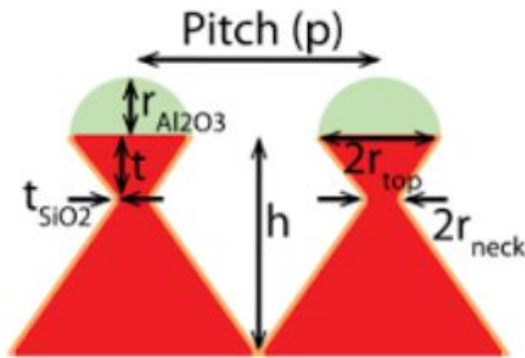
Figure 1: Diagram of the parameterized dimensions created in CST from Ref. 9.

As this was a periodic nanostructure, the angle of incidence of the light had a significant effect on the reflectance of light as optical grating effects came into play. However, in our analysis we only considered normal incidence due to the substantial increase in required computational time required for other angles of incidence. This was due to the fact that at normal incidence, we could use a single structure rather than a periodic array. Due to the number of simulations that were required, it was not feasible given our resources and time to incorporate a full range of incidence angles in a periodic structure simulation.

The final results for minimized S_{11} were obtained using the optimetric sweep option available in CST over 3 frequency ranges: (1) near-IR (0.75 μm< λ < 1.4 μm), (2) short-wavelength IR (1.4 μm< λ < 3.0 μm), and (3) mid-wavelength IR (3.0 μm< λ < 8.0 μm). We performed this minimization for each range using the four materials (Si/SiO$_2$, InSb, Ge, HgCdTe) previously listed to identify what configuration was optimal for each range.

Prototype

Our project has been fully simulation based, and as such we did not attempt to prototype the cone-and-ball nanostructured surface. However, there is an established self-assembling block copolymer fabrication method that has been successful with Si, as outlined below[9]. As shown in Figure 2, first a solution of cylindrical phase polystyrene block-poly(methyl methacrylate) (PS-b-PMMA) block copolymers with four different molecular weights in a toluene solvent is spin cast onto the substrate and annealed at a fairly low temperature (205 ℃) for 12 hours. The annealed block copolymer film is then infiltrated with aluminum (Al) by exposure to tri-methyl aluminum (TMA) and water vapor in an atomic layer deposition system to form the Al$_2$O$_3$ spheres on the substrate surface. The cones are then selectively vertically etched below the alumina spheres by an inductively coupled plasma (ICP) reactive ion etch (RIE) of a 50:50:10 ratio of HBr, Cl$_2$, and O$_2$. To apply this method to materials that are preferred for IR frequencies, this dry etching chemistry must be tailored to the material. For InSb, HgCdTe, and Ge, ICP RIE have been shown to be able to define highly anisotropic features with CH$_4$/H$_2$/Ar (1), Ar (2) or CH$_4$/H$_2$ (3), and CF$_4$ (4) plasmas, respectively[14-17]. If time had permitted, this prototyping could have been done in the Nanocenter FabLab with the aid of the FabLab staff.
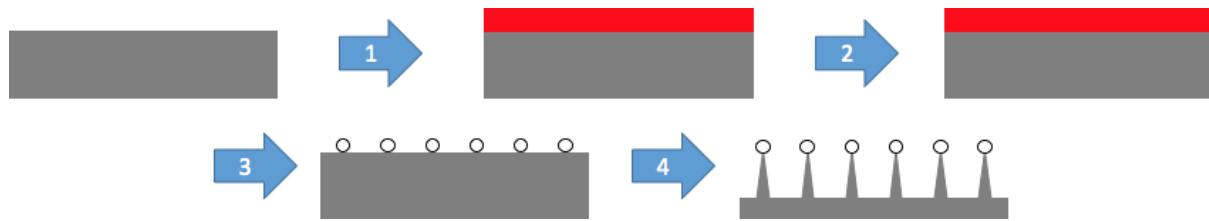
Figure 2: Schematic showing the hypothetical prototyping steps: (1) Spin cast PS-b-PMMA solution (red) on substrate (grey); (2) annealing of polymer solution; (3) Al_2O_3 hemispheres (white) fabricated by exposure to TMA and water vapor; (5) ICP RIE to form final cone-and-ball structures.

Ethical and Environmental Impact

The ethical impact of this proposed design and its applications varies significantly from design to prototyping to production. Our successful design includes inherent benefits, such as contributing to the scientific knowledge base. If the design proceeds to production, the potential benefits of these nanostructures include higher performing solar cells, more efficient fiber optic cables, and more sensitive night vision and sensor systems. It is important to note that the majority of these societal benefits would be realized only if production is very successful.

The environmental impact of our design will increase the closer it comes to production. During the design phase, no environmental costs were incurred beyond the energy needed to run the multi-processor workstation computer that runs the CST simulation software. Fortunately, the University of Maryland partially generates its own power using a Combined Heat and Power (CHP) natural gas turbine system. This ensures the best possible efficiency from a conventional hydrocarbon fuel source. The 2015 University of Maryland Sustainability report notes that this system provides 90% of the energy used by the campus during the winter, and 50% of the energy used by the campus during the summer[18].

Although our design is successful, we do not have the time to move into prototyping. If we did have time, the University of Maryland has fantastic on-site facilities for microprocessing, and the FabLab is a responsibly managed, fully-featured clean room. Waste is properly tagged and disposed of, and even though the prototyping could take months the overall process would not create a novel impact on the existing FabLab procedures[19].

With a successful prototype, we could look into getting a patent and possibly licensing the technology to a larger semiconductor manufacturer. This is where the environmental costs start to become significant. Silicon increases in value by five orders of magnitude (per kg) during the refinement process, and each step has lower yields[20]. In addition, some of the materials we studied, like HgCdTe, contain toxic elements and would not be suitable for applications where erosion of the IR-antireflection layer is possible even though they have very good properties for IR absorption. Overall energy consumption is significant for any scaled up process, and while the nano-geometry in question uses vanishingly small amounts of any given substance, the precursors and solutions required for deposition are often extremely toxic. A proper life cycle analysis would be a good idea at this point to see at what scale the technology's widespread benefits outweigh its costs.

Intellectual Merit

Throughout this project, we have learned about the optical behavior of the cone-and-ball Si and Al_2O_3 nanostructure in the near IR wavelength range. To the best of our knowledge, the optical properties of our cone-and-ball structure in the IR spectrum had not been simulated nor demonstrated experimentally. Using simulation, we determined the effect of structure density and size on the amount of reflection from the nanostructure array. By doing so, we investigated the applicability of the Si-Al_2O_3 nanostructures in a variety of situations such as astronomical instruments and photovoltaic devices[21,22]. Photovoltaic devices are a popular predicted application of IR absorbing nanostructures, since a minimized reflectance would allow for greater efficiency in absorbing light[12].

This project focused on an analysis of the impact of geometry on the absorption of IR radiation. Since several materials were tested, we did not intend to find the ideal combination of a material, geometry, and wavelength. Rather, we analyzed the interaction between geometry and absorption for several materials in the near and short-wavelength IR. We compared the optimal reflectance for four materials and their respective geometries, and this can later be used in future development of IR-antireflection nanostructures depending on what materials are most suitable for the application. We also compared the behavior of these nanostructures with silicon structures optimized for visible light, as well as seeing how our structures and the silicon structures behaved in the IR spectrum.

Broader Impact

Moth's-eye nanostructures can decrease the reflectance and increase the proficiency of devices that are optimized for visible and short-wavelength to near IR applications. Silicon has applications in the visible range of the spectrum for devices such as solar cells[5]. The other materials we simulated have applications in the IR region including forward looking infrared (FLIR) detectors, and IR astronomical telescopes[8,22]. Improving the performance of such devices can increase our knowledge of our universe and increase the widespread use of terrestrial solar cells. The upcoming James Webb space telescope views the cosmos in unprecedented detail in the long-visible and short-wavelength to mid-wavelength IR range, and our antireflective coating design could lead to higher performance for subsequent space telescopes.

In addition to the the technical impact of our project, the educational benefits are also apparent. Through this project, our diverse team - despite many members lacking simulation experience - gained the confidence to work with simulations and data management. This design project has helped forge us into young scientists and engineers, and the lessons that we have learned will continue to be beneficial throughout our careers.

Results and Discussion

Silicon Nanostructure
We created a silicon nanostructure in CST both to compare our simulation results to literature data and to study the behavior of the silicon nanostructure in the IR range. For our simulation data to be usable, our results had to match within 10% of the measured reflectance found by Rahman et

al. for each set of nanostructure dimensions. More importantly, the trend of each S_{11} curve must be similar to that of the respective measured reflectance curve. The results of our simulations compared to the reflectance measured by Rahman et al. for each geometry denoted by the cone height, are shown in Figure 3.
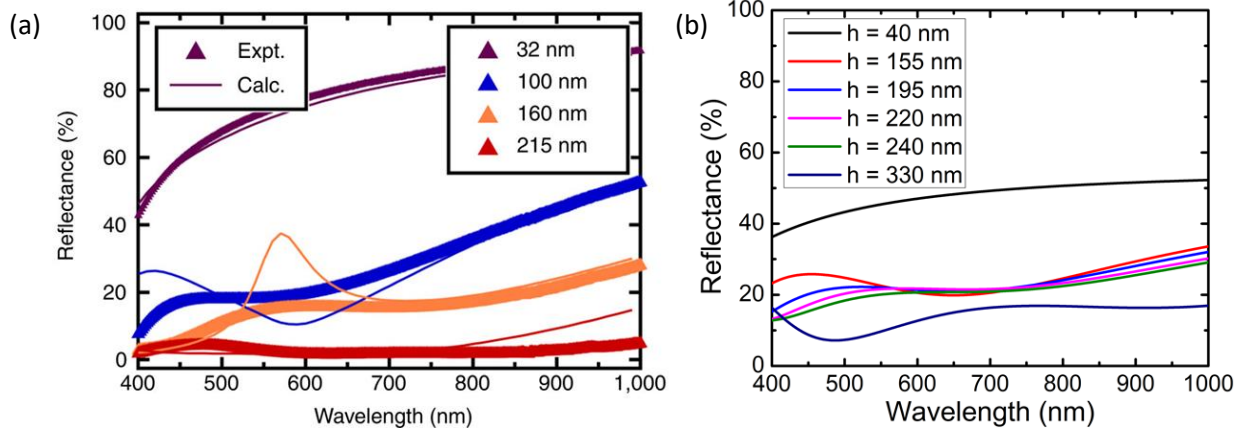

Figure 3: (a) The reflectance of nanocones of varying heights from Ref. 9.
(b) The results of our simulation using the geometry given by Rahman et al. Also shown is the reflectance of an optimized silicon nanostructure.

As seen in Figure 3, the measured reflectance and S_{11} simulation values match within 5% at a wavelength of 400 nm but differs by up to 10% as the wavelength approaches 1000 nm. This may be because CST uses primarily optical constants instead of optical functions in its calculations and these optical constants may be more accurate for shorter wavelengths. The trend for each nanostructure geometry did match that of the measured reflectance, with troughs found around 700 nm for both the 160 nm-high geometry measured reflectance and the 155 nm-high geometry S_{11}. Likewise, both the 32 nm-high geometry measured reflectance and the 40 nm-high geometry S_{11} curve display a logarithmic behavior. Thus, we were able to proceed with our simulations.

To further study the behavior of the cone-and-ball nanostructure in the visible spectrum, we ran an optimization program in CST to determine the optimal geometry for a silicon-based structure in the visible spectrum. The results of this optimization are shown in Figure 3 as h = 330 nm. The optimized geometry was able to achieve an S_{11} of under 20%, a significant improvement from the planar silicon reflectance of more than 40%, as seen in Figure 5.

While the bandgap of silicon (1.3 eV) limits it from any absorption applications in the IR range, silicon can still be used for IR applications where only transmittance is necessary, such as in space telescopes. In this case, geometric effects arising from refraction across the air/Si interface and light trapping within the structures instead of absorption by the material will reduce the reflectance from the surface. For this reason, we also ran simulations for the silicon nanostructure past its bandgap into the IR spectrum. As seen in Figure 4, the reflectance remains below that of planar silicon in the near, short-wavelength, and some of the mid-wavelength IR range. This suggests the nanostructures are too short to effectively alter the surface reflectance of the silicon wafer in the long-wavelength and some of the mid-wavelength IR. We took this observation into account when designing our nanostructures for IR applications and limited our optimizations to the near and short-wavelength IR.
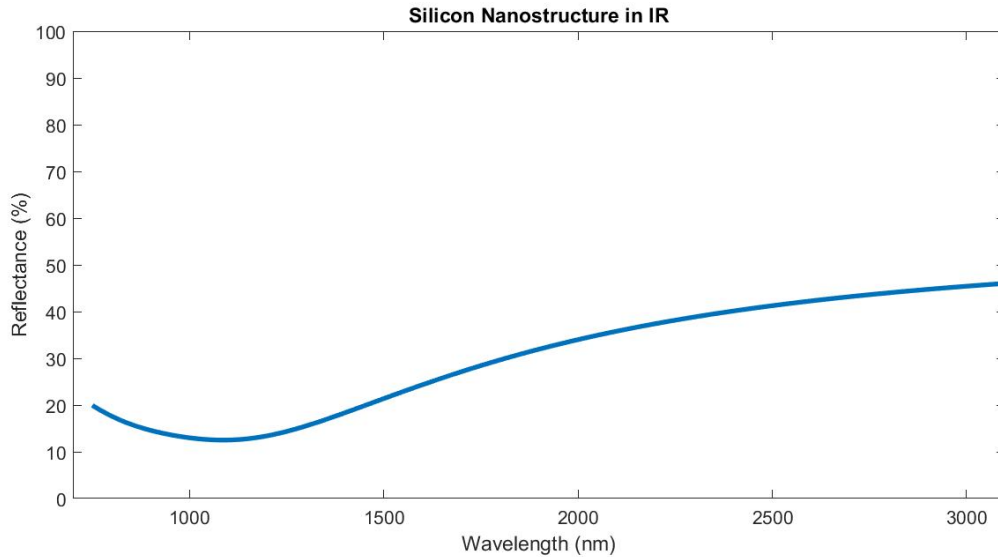
Figure 4: Reflectance vs. wavelength of silicon nanostructure in IR spectra.

Nanostructures for Infrared Applications: InSb, Germanium, HgCdTe

To determine the best material for near IR and short-wavelength IR applications, we simulated six materials: four compounds of HgCdTe, Ge, and InSb. We optimized each one for near IR and for short-wavelength IR. Additionally, we simulated planar substrates of each material across the near and short-wavelength IR spectra in order to make a definitive comparison between the nanostructure and substrate. As shown in Figure 5, the reflectance of the substrates in the near and short-wavelength IR spectra is within 50% to 60%.
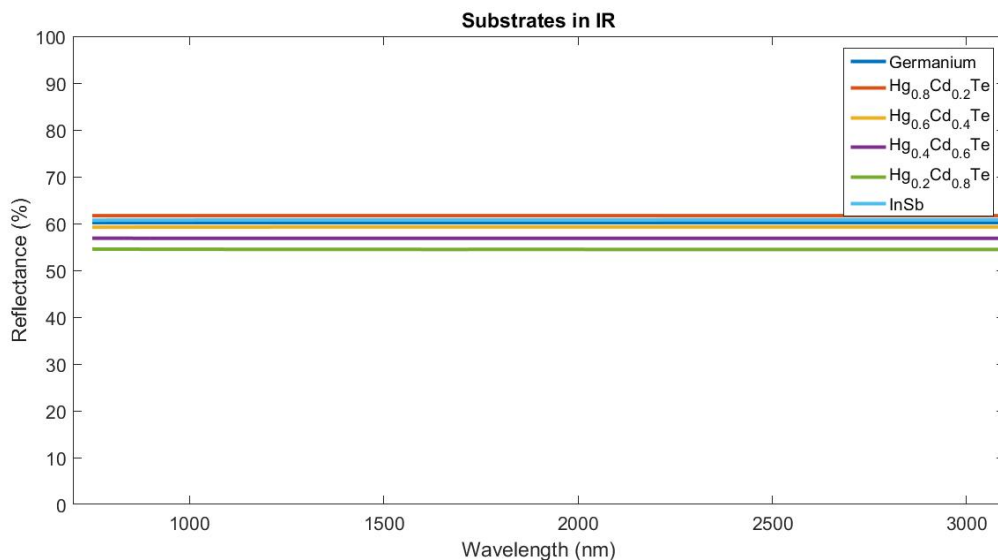
Figure 5: Reflectance vs. wavelength of planar HgCdTe, Germanium, and InSb in IR spectra.

Compounds with the formula $Hg_{1-x}Cd_xTe$ have different properties for different values of x. In our case, these different compounds have different reflectance properties. The reflectance properties of optimized cone-and-ball nanostructures of $Hg_{1-x}Cd_xTe$ compounds with x values of 0.2, 0.4, 0.6, and 0.8 in the short-wavelength and near IR are shown in Figures 6a and 6b respectively.
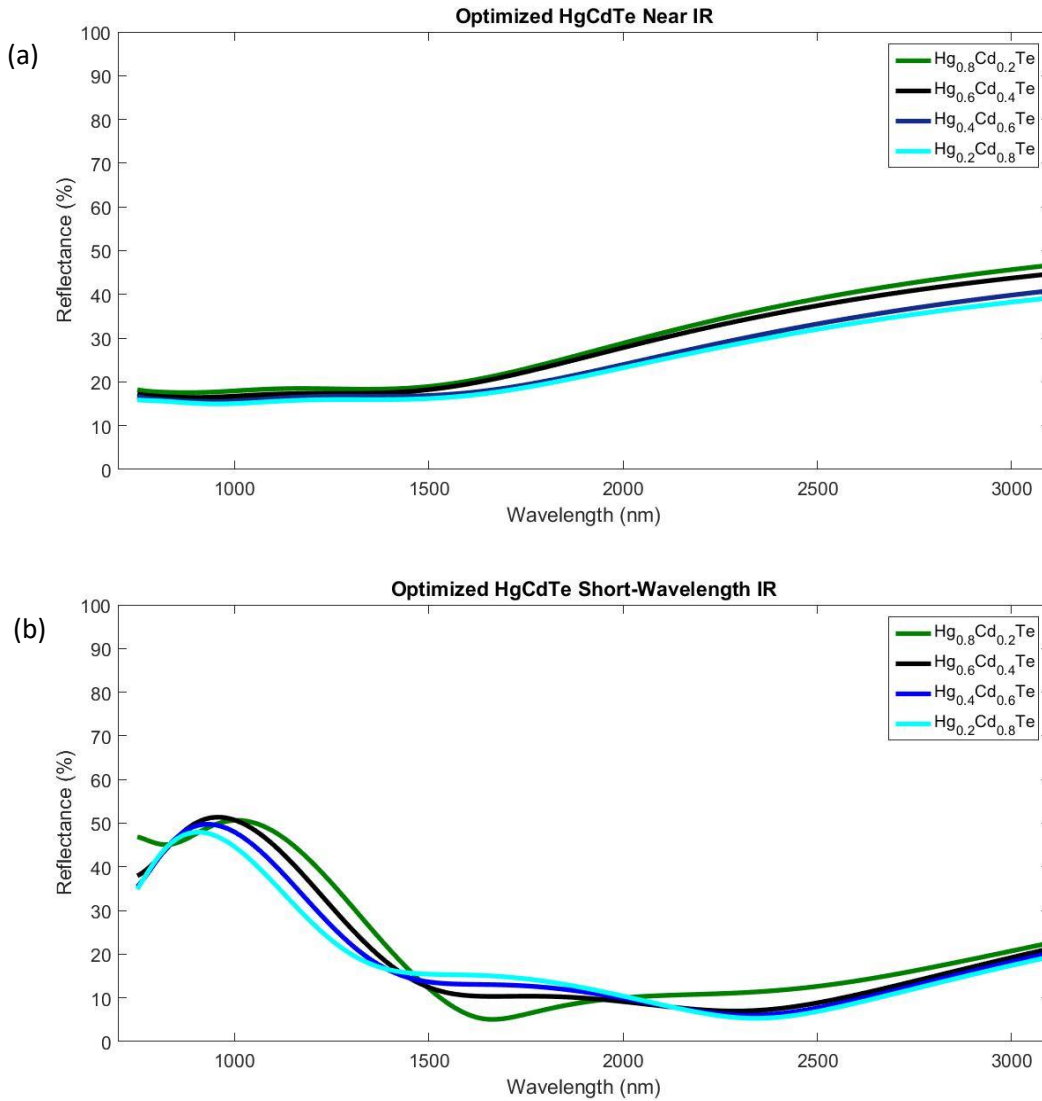
Figure 6: (a) Reflectance vs. wavelength of the HgCdTe compounds for each geometry optimized for the near IR. (b) Reflectance vs. wavelength of the HgCdTe compounds for each geometry optimized for the short-wavelength IR.

In both the short-wavelength and near IR, the HgCdTe compound with x=0.8 had the lowest reflectance values. From this point on, only $Hg_{0.2}Cd_{0.8}Te$ was considered in the simulations.

Using CST, we were able to optimize the cone-and-ball nanostructure specifically for near IR (0.75 μm-1.4 μm) and short-wavelength IR (1.4 μm-3 μm) spectra. The reflectance results from these optimization runs are shown in Figures 7a and 7b respectively. The dimensions of the optimized cone-and-ball nanostructure for each of the three materials are shown in Tables 1a and 1b where the dimensions are all in nanometers.
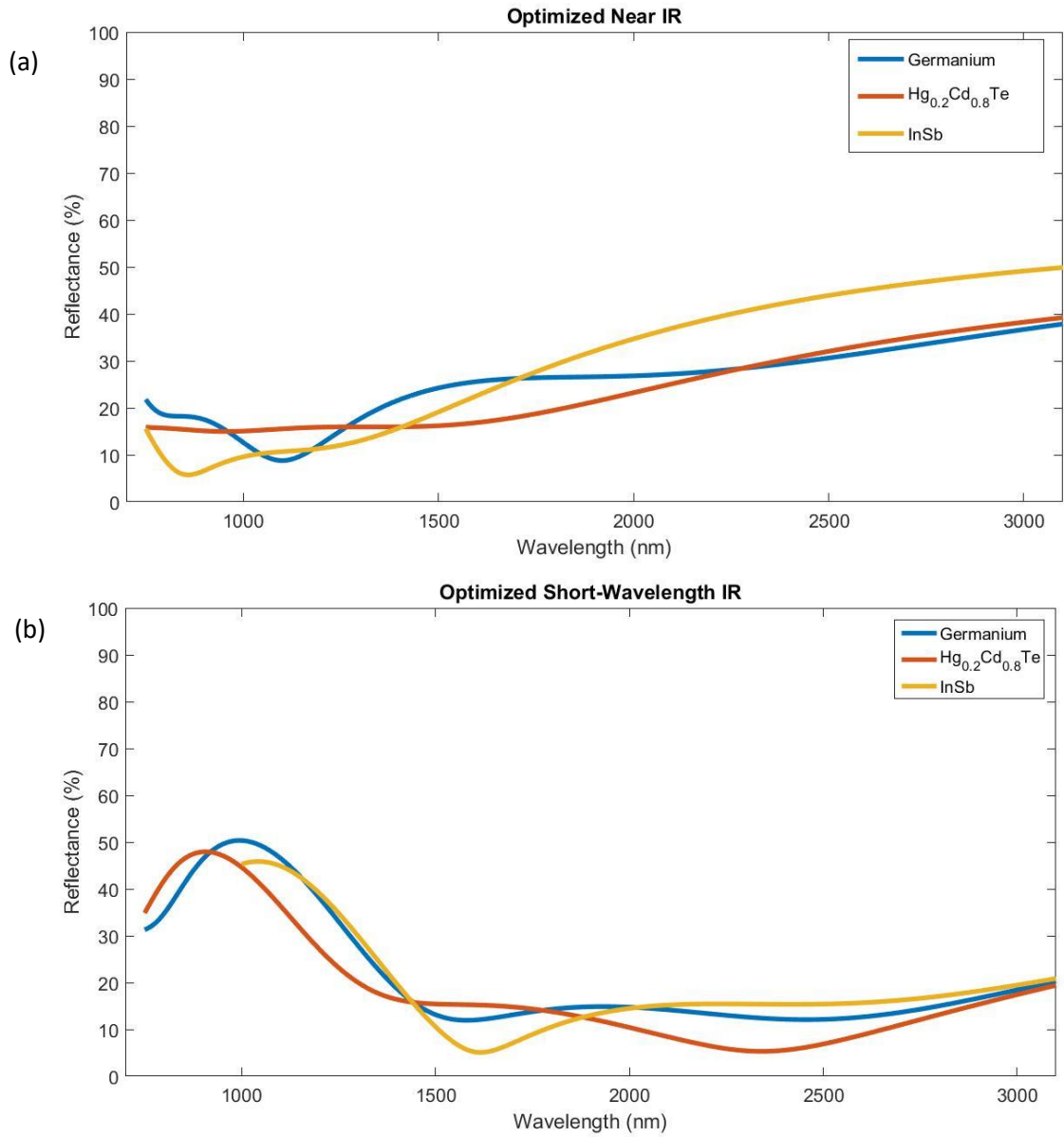
Figure 7: (a) Reflectance vs. wavelength for the three materials optimized for the near IR. **(b)** Reflectance vs. wavelength for the three materials optimized for the short-wavelength IR.

Optimized Near IR Dimensions (nm)			
Material	Ge	$Hg_{0.2}Cd_{0.8}Te$	InSb
Height	359.1	459.2	228.5
pitch	43.27	48.2	32.67
r_{head}	13.74	15.26	11.5
r_{neck}	15.09	6.488	11.23
t	7.108	3.954	2.46

Optimized Short-Wavelength IR Dimensions (nm)			
Material	Ge	$Hg_{0.2}Cd_{0.8}Te$	InSb
Height	430.5	428.7	449.1
pitch	35.35	26.06	37.5
r_{head}	13.27	13.27	15
r_{neck}	12.84	9.223	13.7
t	5.322	1	6.1

Table 1: (a) The dimension of the optimized geometry for the near IR for each material. (b) The dimension of the optimized geometry for the short-wavelength IR for each material.

These results show that by changing the structure using a different processing method, different properties can be achieved depending on the application. It is interesting to note that for the near IR the InSb nanostructure is the smallest but for the short-wavelength IR the InSb is the largest. For both the near IR and short-wavelength IR ranges, the optimized InSb had the lowest average reflectance. However, it is important to note that for all six materials simulated and optimized in both the near IR and short-wavelength IR spectra, the reflectance was lowered to less than 20%. This is considerably less than the reflectances simulated for planar substrates of these materials as was shown in Figure 5 above. Considering the wide range of optical properties in the six materials, this implies that the nanostructure can be applied to most materials as long as the geometry can be accurately produced using the microprocessing methods mentioned in the prototype section.

Conclusion

In closing, we have optimized, by simulation, Si cone-and-ball nanostructured surfaces for use in the visible light regime, and have optimized the same cone-and-ball structures in the short-wavelength and near IR regions for InSb, HgCdTe, and Ge as well. For each material, we have a maximum reflectance value around 20%, similar to experimental results from previous literature work[9]. These nanostructured surfaces could have applications in night vision, IR detectors, and IR telescopes where in each application, the surface could significantly reduce the reflectance and improve the performance of the device. Finally, the next steps for the project would be to fabricate the structures by combining self-assembling block copolymer templates and highly anisotropic plasma etching tailored to each material.

Future Work

Our current project can be seen as a proof of concept. We have shown that the moth's eye nanostructure can be applied to the near and short-wavelength IR ranges in order to achieve minimal reflectance values when compared to just a planar substrate. This project specifically explored the materials Si, InSb, Ge, and HgCdTe. If allowed more time, we would have liked to explore materials such as lead glass and gallium arsenide, materials that are commonly used for night vision applications. Since our model is completely parameterized, it is versatile can be applied to a wide variety of materials as long as it can be fabricated in a lab. Additionally, we would have liked to explore more angles of incidence. The only angle we considered was 90°

because this is the angle at which maximum reflectance is achieved. At other angles of incidence, it is likely that we would get smaller reflectance values.

Due to limitations of the software we used optical constants rather than functions to characterize our reflectance. Moving forward, we would like to use a more powerful software package so that we can implement dielectric functions. After running several simulations, we would like to test the models in the lab by fabricating a prototype. We would create a test structure as outlined in the prototype section. This step would obviously require a lot more time and money. However, it would provide us with the opportunity to test our models against observed lab data, further verifying our simulation runs.

Acknowledgements

References

1   Stoykovich, M. P. & Nealey, P. F. Block copolymers and conventional lithography. *Materials Today* **9**, 20-29, doi:http://dx.doi.org/10.1016/S1369-7021(06)71619-4 (2006).

2   Dellieu, L., Sarrazin, M., Simonis, P., Deparis, O. & Vigneron, J. P. A two-in-one superhydrophobic and anti-reflective nanodevice in the grey cicada *Cicada orni* (Hemiptera). *J. Appl. Phys.* **116** (2014).

3   Huang, Y.-F. *et al.* Improved broadband and quasi-omnidirectional anti-reflection properties with biomimetic silicon nanostructures. *Nat Nano* **2**, 770-774 (2007).

4   Honsberg, C. & Bowden, S. *Anti-Reflection Coating*, <http://www.pveducation.org/pvcdrom/design/anti-reflection-coatings> (

5   Lazo, J. *Moth-Eye-Inspired Nanostructure Boosts Tandem Solar Cells' Performance*, <http://www.greenoptimistic.com/moth-eye-inspired-nanostructure-boosts-tandem-solar-cells-performance-20121120/#.VsuP2fIrKhc> (2012).

6   Diedenhofen, S. L. *et al.* Broad-band and Omnidirectional Antireflection Coatings Based on Semiconductor Nanorods. *Advanced Materials* **21**, 973-978, doi:10.1002/adma.200802767 (2009).

7   Park, K.-C. *et al.* Nanotextured Silica Surfaces with Robust Superhydrophobicity and Omnidirectional Broadband Supertransmissivity. *ACS Nano* **6**, 3789-3799, doi:10.1021/nn301112t (2012).

8   Yang, K., Wang, L. & Zhang, Q. Preparation and properties of a flexible night vision imaging system filter for avionic LED displays. *Journal of Materials Science: Materials in Electronics* **26**, 2222-2229, doi:10.1007/s10854-015-2672-5 (2015).

9   Rahman, A. *et al.* Sub-50-nm self-assembled nanotextures for enhanced broadband antireflection in silicon solar cells. *Nat Commun* **6** (2015).

10   Zens, T., Becla, P., Agarwal, A. M., Kimerling, L. C. & Drehman, A. Long wavelength infrared detection using amorphous InSb and InAs0.3Sb0.7. *Journal of Crystal Growth* **334**, 84-89, doi:http://dx.doi.org/10.1016/j.jcrysgro.2011.08.016 (2011).

11   Fowles, G. R. *Introduction to Modern Optics*. (Courier Corporation, 1975).

12   Han, K. & Chang, C.-H. Numerical Modeling of Sub-Wavelength Anti-Reflective Structures for Solar Module Applications. *Nanomaterials* **4**, doi:10.3390/nano4010087 (2014).

13   Kasap, S. & Capper, P. *Springer Handbook of Electronic and Photonic Materials*. 54 (Springer, 2007).

14   Pusino, V., Xie, C., Khalid, A., Thayne, I. G. & Cumming, D. R. S. Development of InSb dry etch for mid-IR applications. *Microelectronic Engineering* **153**, 11-14, doi:http://dx.doi.org/10.1016/j.mee.2015.12.014 (2016).

15   Perera, D., Pattison, J. & Wijewarnasuriya, P. Minimizing Reflectivity by Etching Microstructures in Mercury Cadmium Telluride (HgCdTe). (Army Research Lab, 2013).

16   Srivastav, V., Pal, R. & Vyas, H. P. Overview of etching technologies used for HgCdTe. *Opto-Electronics Review* **13**, 197-211 (2005).

17   Shim, K.-H. *et al.* Nanoscale dry etching of germanium by using inductively coupled CF4 plasma. *Electronic Materials Letters* **8**, 423-428, doi:10.1007/s13391-012-1109-z (2012).

18   Progress Report: Carbon Neutrality. (University of Maryland, Sustainable UMD 2015).

19   Colvin, V. L. The potential environmental impact of engineered nanomaterials. *Nat Biotech* **21**, 1166-1170 (2003).

20   Plepys, A. in *Electronics and the Environment, 2004. Conference Record. 2004 IEEE International Symposium on.* 159-165.

21   Zhang, Y. & Xuan, Y. Biomimetic omnidirectional broadband structured surface for photon management in photovoltaic–thermoelectric hybrid systems. *Solar Energy Materials and Solar Cells* **144**, 68-77, doi:http://dx.doi.org/10.1016/j.solmat.2015.08.035 (2016).

22   Imada, H. *et al.*   84502F-84502F-84509.